J. Fluid Mech. (2015), *vol.* 784, R2, doi:10.1017/jfm.2015.606

JFM RAPIDS
journals.cambridge.org/rapids

The asymptotic equivalence of fixed heat flux and fixed temperature thermal boundary conditions for rapidly rotating convection

Michael A. Calkins[1,†], Kevin Hale[2], Keith Julien[1], David Nieves[1], Derek Driggs[1] and Philippe Marti[1]

[1]Department of Applied Mathematics, University of Colorado, Boulder, CO 80309, USA

[2]Harvey Mudd College, Claremont, CA 91711, USA

(Received 21 July 2015; revised 25 September 2015; accepted 15 October 2015;
first published online 4 November 2015)

The influence of fixed temperature and fixed heat flux thermal boundary conditions on rapidly rotating convection in the plane layer geometry is investigated for the case of stress-free mechanical boundary conditions. It is shown that whereas the leading-order system satisfies fixed temperature boundary conditions implicitly, a double boundary layer structure is necessary to satisfy the fixed heat flux thermal boundary conditions. The boundary layers consist of a classical Ekman layer adjacent to the solid boundaries that adjust viscous stresses to zero, and a layer in thermal wind balance just outside the Ekman layers that adjusts the normal derivative of the temperature fluctuation to zero. The influence of these boundary layers on the interior geostrophically balanced convection is shown to be asymptotically weak, however. Upon defining a simple rescaling of the thermal variables, the leading-order reduced system of governing equations is therefore equivalent for both boundary conditions. These results imply that any horizontal thermal variation along the boundaries that varies on the scale of the convection has no leading-order influence on the interior convection, thus providing insight into geophysical and astrophysical flows where stress-free mechanical boundary conditions are often assumed.

Key words: convection, geophysical and geological flows, quasi-geostrophic flows

1. Introduction

One of the simplest and most commonly studied systems for investigating convection dynamics is the so-called Rayleigh–Bénard configuration, consisting of a Boussinesq fluid layer of depth H confined between plane-parallel boundaries, and heated from below. The constant gravity vector $\boldsymbol{g} = -g\hat{\boldsymbol{z}}$ points vertically downwards.

† Present address: Department of Physics, University of Colorado, Boulder, CO 80309, USA.

Two limiting cases for thermal boundary conditions are often considered when posing the problem mathematically: (1) 'perfectly conducting', or fixed temperature (FT), boundary conditions in which the temperature is held fixed along the bounding surfaces; and (2) 'perfectly insulating', or fixed flux (FF), boundary conditions in which the normal derivative of the temperature is fixed at the boundaries (e.g. Chapman & Proctor 1980). Thermal boundary conditions of geophysical and astrophysical relevance are often considered to reside somewhere between these fixed flux and fixed temperature limits.

For a Newtonian fluid of constant thermal expansivity α, kinematic viscosity ν and thermal diffusivity κ, the non-dimensional Rayleigh number quantifies the strength of the buoyancy force. For the FT and the FF cases we have respectively

$$Ra_{FT} = \frac{\alpha g \Delta T H^3}{\nu\kappa}, \quad Ra_{FF} = \frac{\alpha g \beta H^4}{\nu\kappa}, \tag{1.1a,b}$$

where ΔT is the fixed temperature difference between the top and bottom boundaries and β is the fixed temperature gradient maintained at the boundaries. The Prandtl number quantifies the relative importance of viscous and thermal diffusion as $Pr = \nu/\kappa$. Upon defining the non-dimensional measure of heat transfer via the Nusselt number,

$$Nu = \frac{\text{total heat transfer}}{\text{conductive heat transfer}} = \frac{\beta H}{\Delta T}, \tag{1.2}$$

it is straightforward to show that the two Rayleigh numbers defined above are related simply by $Ra_{FF} = NuRa_{FT}$. We thus see that for linear convection in which $Nu \equiv 1$ the two Rayleigh numbers are equivalent. For nonlinear convection in which the critical Rayleigh number has been surpassed, $Nu > 1$ is achieved by adjustment of the temperature gradient β at fixed ΔT for FT boundaries, and *vice versa* for FF boundaries.

Linear stability shows that for the case of non-rotating convection the most unstable wavenumber is finite for FT boundary conditions (e.g. Chandrasekhar 1961), but is zero for FF boundary conditions (Hurle, Jakeman & Pike 1967). The two-dimensional numerical simulations of Johnston & Doering (2009) showed that the statistics for the two cases converge as the Rayleigh number is increased and the flow becomes turbulent. It is now generally believed that this result also holds in three-dimensional convection simulations when sufficient numerical resolution is employed (e.g. see Ahlers, Grossman & Lohse 2009).

When the system is rotating with rotation vector $\boldsymbol{\Omega} = \Omega\widehat{\boldsymbol{z}}$, the Ekman number, $E_H = \nu/2\Omega H^2$, is an additional non-dimensional number required to specify the strength of viscous forces relative to the Coriolis force. In this paper we are concerned with the rapidly rotating quasi-geostrophic convection limit defined by $E_H \to 0$ and $Ro_c = \sqrt{Ra/Pr}E_H \ll 1$, where Ro_c is the convective Rossby number and Ra denotes either Ra_{FT} or Ra_{FF} depending upon the particular boundary conditions employed (e.g. Julien *et al.* 1996; Liu & Ecke 1997; Sprague *et al.* 2006). Accessing the rapidly rotating regime continues to be challenging for both laboratory experiments and numerical simulations due to mechanical and computational limitations, respectively (Stevens, Clercx & Lohse 2013; Ecke & Niemela 2014; Stellmach *et al.* 2014; Cheng *et al.* 2015). As of the writing of this paper, only two investigations of FF boundary conditions for the rotating plane layer geometry have been published in the literature, with Dowling (1988) and Takehiro *et al.* (2002) examining the weakly rotating and rapidly rotating linear cases respectively. Takehiro *et al.* (2002) utilized a modal

truncation approach to show that the critical parameters for the two cases should converge as $E_H \to 0$; the present work confirms this suggestion.

In the present work we distinguish between 'interior' and 'boundary layer' dynamics, and show that the interior governing equations are identical for the two different thermal boundary conditions upon a simple rescaling of the Rayleigh number and temperature. Because the $E_H \to 0$ limit is a singular perturbation of the governing equations, the interior equations cannot satisfy the FF boundary conditions at leading order; a double boundary layer structure is necessary to adjust both the horizontal viscous stresses and the normal derivative of the temperature fluctuation to zero (cf. Heard & Veronis 1971). It is shown that the boundary layer corrections are asymptotically weak, however, showing that to leading order the interior quasi-geostrophic convection dynamics are equivalent for both thermal boundary conditions.

In § 2 we present the linear stability of the full Boussinesq Navier–Stokes equations. In § 3 we present the asymptotic reduction of the Navier–Stokes equations in the rapidly rotating limit. Concluding remarks are given in § 4.

2. Linear stability of the Navier–Stokes equations

In this section we briefly present the linear stability of the Boussinesq Navier–Stokes equations for both FT and FF thermal boundary conditions. Upon scaling lengths with the depth of the fluid layer H and time with the viscous diffusion time H^2/ν, the linear system becomes

$$\partial_t \boldsymbol{u} + \frac{1}{E_H}\widehat{\boldsymbol{z}} \times \boldsymbol{u} = -\frac{1}{E_H}\boldsymbol{\nabla} p + \frac{Ra}{Pr}\vartheta' \widehat{\boldsymbol{z}} + \nabla^2 \boldsymbol{u}, \tag{2.1}$$

$$\partial_t \vartheta' - w = \frac{1}{Pr}\nabla^2 \vartheta', \tag{2.2}$$

$$\boldsymbol{\nabla} \cdot \boldsymbol{u} = 0, \tag{2.3}$$

where the velocity vector is denoted by $\boldsymbol{u} = (u, v, w)$, and the temperature is decomposed into mean and fluctuating variables according to $\vartheta = \overline{\vartheta} + \vartheta'$. For both sets of thermal boundary conditions $\overline{\vartheta} = 1 - z$, and the fluctuating thermal boundary conditions therefore become

$$\vartheta' = 0, \quad \text{at } z = 0, 1 \quad \text{(FT)} \tag{2.4}$$

$$\partial_z \vartheta' = 0, \quad \text{at } z = 0, 1 \quad \text{(FF)}. \tag{2.5}$$

Stress-free impenetrable mechanical boundary conditions on the top and bottom boundaries are assumed throughout and are given by

$$w = \partial_z u = \partial_z v = 0, \quad \text{at } z = 0, 1. \tag{2.6}$$

The system (2.1)–(2.3) is discretized in the vertical and horizontal dimensions with Chebyshev polynomials and Fourier modes respectively, and formulated as a generalized eigenvalue problem. We solve the system in primitive variable form and enforce boundary conditions via the tau method. The eigenvalue problem is solved with Matlab's 'sptarn' function. For further details of the numerical methods the reader is referred to Calkins, Julien & Marti (2013).

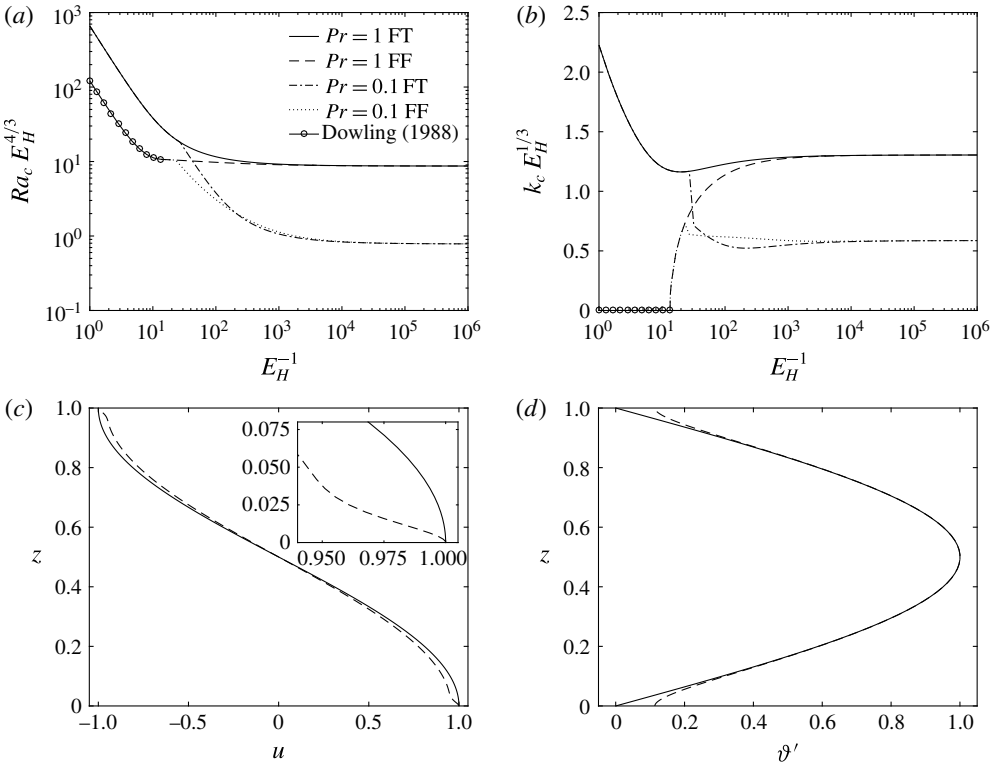

FIGURE 1. Linear stability of the Navier–Stokes equations for fixed temperature (FT) and fixed flux (FF) thermal boundary conditions. (*a*) Asymptotically scaled critical Rayleigh number and (*b*) critical wavenumber as a function of the inverse Ekman number for both steady ($Pr = 1$) and oscillatory ($Pr = 0.1$) convection. (*c*) Horizontal velocity and (*d*) temperature eigenfunctions for $Pr = 1$ and $E_H = 10^{-4}$; the inset figure in (*c*) shows a magnified view of the Ekman layer along the bottom boundary. In (*a*) and (*b*) the solid line with open circles shows values calculated from the explicit formula of Dowling (1988).

Figure 1 shows results from the linear stability calculations. Results are given for both steady ($Pr = 1$) and oscillatory ($Pr = 0.1$) convection; we note that oscillatory convection does not exist for $Pr \geqslant 1$ and becomes the primary instability for $Pr \lesssim 0.68$ (Chandrasekhar 1961). For $E_H \lesssim 10^{-5}$, both the asymptotically scaled critical Rayleigh number $Ra_c E_H^{4/3}$ (figure 1*a*) and the wavenumber $k_c E_H^{1/3}$ (figure 1*b*) obtained from FT and FF boundary conditions are observed to converge to nearly equivalent values. For $E_H = 10^{-6}$, for instance, the differences in the critical parameters for the two cases are found to be $\ll 1\,\%$. The solid line with open circles shows values calculated from the explicit formula of Dowling (1988) for which the instability is characterized by $k_c = 0$.

Figure 1(*c*) shows the horizontal (x) velocity eigenfunction for $E_H = 10^{-4}$, where Ekman layers can be seen at the top and bottom boundaries for the FF (dashed curve) case; a magnified view of the bottom Ekman layer is shown in the inset figure. The temperature perturbation eigenfunctions plotted in figure 1(*d*) show that both the FT and FF cases have identical structure in the fluid interior, whereas the two profiles differ significantly near the top and bottom boundaries. In the following section we

present the asymptotic reduction of the Navier–Stokes equations to better understand and quantify this behaviour.

3. Asymptotics

To proceed with the asymptotic development, we follow the work of Sprague *et al.* (2006) and write the governing equations using a generic non-dimensionalization such that

$$D_t \boldsymbol{u} + \frac{1}{Ro}\widehat{\boldsymbol{z}} \times \boldsymbol{u} = -Eu\boldsymbol{\nabla} p + \Gamma\theta\widehat{\boldsymbol{z}} + \frac{1}{Re}\nabla^2\boldsymbol{u}, \tag{3.1}$$

$$\boldsymbol{\nabla}\cdot\boldsymbol{u} = 0, \tag{3.2}$$

$$D_t\vartheta = \frac{1}{Pr\,Re}\nabla^2\vartheta, \tag{3.3}$$

where $D_t(\cdot) = \partial_t(\cdot) + \boldsymbol{u}\cdot\boldsymbol{\nabla}(\cdot)$ and the velocity, pressure and temperature are denoted by $\boldsymbol{u}$, p and ϑ respectively. The above system has been non-dimensionalized utilizing the velocity scale U, length L, time L/U, pressure P and temperature $\widetilde{T}$. For the FT and FF cases the temperature scale becomes ΔT and $Nu\Delta T$ respectively. The Rossby, Euler, buoyancy and Reynolds numbers are defined by

$$Ro = \frac{U}{2\Omega L}, \quad Eu = \frac{P}{\rho_0 U^2}, \quad \Gamma = \frac{g\alpha\widetilde{T}L}{U^2}, \quad Re = \frac{UL}{\nu}. \tag{3.4a–d}$$

In the present work we are interested in the $\epsilon \equiv Ro \to 0$ limit. In the fluid interior we employ multiple scales in the axial space direction and time such that

$$\partial_z \to \partial_z + \epsilon\partial_Z, \quad \partial_t \to \partial_t + \epsilon^2\partial_\tau, \tag{3.5a,b}$$

where $Z = \epsilon z$ is the large-scale vertical coordinate and $\tau = \epsilon^2 t$ is the 'slow' time scale. It has been shown that the following distinguished limits can be taken to reduce the governing equations to accurately model quasi-geostrophic convection (e.g. Sprague *et al.* 2006):

$$Eu = \frac{1}{\epsilon^2}, \quad \Gamma = \frac{\widetilde{\Gamma}}{\epsilon}, \quad Re = O(1), \quad Pr = O(1), \tag{3.6a–d}$$

where $\widetilde{\Gamma} = O(1)$. On scaling the velocity viscously such that $U = \nu/L$ we have

$$\epsilon = E_H^{1/3}, \quad \widetilde{\Gamma} = \frac{E_H^{4/3}Ra}{Pr}, \quad Re = 1, \tag{3.7a–c}$$

where we note that L is the characteristic horizontal scale of convection and behaves as $L = HE_H^{1/3}$ in the limit of rapid rotation (Chandrasekhar 1961). Notably, this L scaling can be derived from the linear axial vorticity equation by assuming a balance between axial vortex stretching and horizontal viscous diffusion. In dimensional terms, this becomes $2\Omega\partial_z w \approx \nu\nabla^2\zeta$, or $2\Omega U/H \sim \nu U/L^3$, where $\zeta = \widehat{\boldsymbol{z}}\cdot\boldsymbol{\nabla}\times\boldsymbol{u}$ is the vertical vorticity; rearranging then yields $L \sim HE_H^{1/3}$. We recall that the notation for the Rayleigh number is generic in the sense that Ra denotes either Ra_{FT} or Ra_{FF}. Hereafter, we define the asymptotically reduced Rayleigh number as $\widetilde{Ra} \equiv E_H^{4/3}Ra = O(1)$. The convective Rossby number then becomes $Ro_c = \epsilon\sqrt{\widetilde{Ra}/Pr}$, and is therefore assumed to be small in the present work.

We utilize a composite asymptotic expansion approach (e.g. Nayfeh 2008) and, following Heard & Veronis (1971), decompose each variable into interior (i), middle (m) and Ekman layer (e) components. For instance, the dependent variable f can be written as

$$f = f^{(i)}(\boldsymbol{x}, Z, t, \tau) + f^{(m)}(x, y, \xi, t) + f^{(e)}(x, y, \eta, t), \tag{3.8}$$

where $\xi = z$ and $\eta = \epsilon^{-1/2} z$ are boundary layer variables. The above representation ensures that each dependent variable is uniformly valid throughout the domain. The boundary layer variables consist of a sum of contributions from the top and bottom boundary layers; for brevity, we focus on the bottom boundary layers. In the present work we make use of the following limits and notation:

$$\lim_{\xi\to\infty}(f^{(m)}) = (f^{(m)})^{(i)} = \lim_{\eta\to\infty}(f^{(e)}) = (f^{(e)})^{(m)} = (f^{(e)})^{(i)} = 0, \tag{3.9}$$

$$\lim_{\xi\to 0}(f^{(i)}) = (f^{(i)})^{(m)} = \lim_{\eta\to 0}(f^{(i)}) = (f^{(i)})^{(e)} = f^{(i)}(Z=0) = f^{(i)}(0). \tag{3.10}$$

We then expand each variable in a power series according to

$$f^{(i)}(\boldsymbol{x}, Z, t) = f_0^{(i)}(\boldsymbol{x}, Z, t, \tau) + \epsilon^{1/2} f_{1/2}^{(i)}(\boldsymbol{x}, Z, t, \tau) + \epsilon f_1^{(i)}(\boldsymbol{x}, Z, t, \tau) + O(\epsilon^{3/2}). \tag{3.11}$$

Each dependent variable is further decomposed into mean and fluctuating components such that

$$f^{(i)}(\boldsymbol{x}, Z, t, \tau) = \overline{f}^{(i)}(Z, \tau) + f'^{(i)}(\boldsymbol{x}, Z, t, \tau), \tag{3.12}$$

where the horizontal averaging operator is defined by

$$\overline{f}(Z, \tau) = \lim_{[\tau],[A]\to\infty} \frac{1}{[\tau][A]} \int_{[\tau],[A]} f \,\mathrm{d}x\,\mathrm{d}y, \quad \text{and} \quad \overline{f'} \equiv 0, \tag{3.13a,b}$$

where A is the small-scale horizontal area.

3.1. *The interior equations*

By substituting decompositions for each variable of the form (3.8) into the governing equations and utilizing the limits (3.9)–(3.10), equations for each region can be derived; expansions of the form (3.11) are then utilized to determine the asymptotic behaviour of each fluid region. Because the derivation of the interior equations has been given many times previously, we present only the salient features and direct the reader to previous work (e.g. Sprague *et al.* 2006) for details on their derivation. The main point is that the interior convection is geostrophically balanced and horizontally divergence-free to leading order,

$$\widehat{\boldsymbol{z}} \times \boldsymbol{u}_0^{(i)} = -\nabla_\perp p_1^{(i)}, \quad \nabla_\perp \cdot \boldsymbol{u}_{0,\perp}^{(i)} = 0, \tag{3.14a,b}$$

where $\nabla_\perp = (\partial_x, \partial_y, 0)$. The above relations allow us to represent the geostrophic velocity via the geostrophic streamfunction $\psi_0^{(i)} \equiv p_1'^{(i)}$ such that $\boldsymbol{u}_{0,\perp}^{(i)} = -\boldsymbol{\nabla} \times \psi_0^{(i)} \widehat{\boldsymbol{z}}$. The vertical vorticity is then $\zeta_0^{(i)} = \nabla_\perp^2 \psi_0^{(i)}$. The interior vertical vorticity, vertical momentum, fluctuating heat and mean heat equations then become

$$D_t^\perp \zeta_0^{(i)} - \partial_Z w_0'^{(i)} = \nabla_\perp^2 \zeta_0^{(i)}, \tag{3.15}$$

$$D_t^\perp w_0'^{(i)} + \partial_Z \psi_0^{(i)} = \frac{\widetilde{Ra}}{Pr} \vartheta_1'^{(i)} + \nabla_\perp^2 w_0'^{(i)}, \tag{3.16}$$

$$D_t^{\perp}\vartheta_1^{\prime(i)} + w_0^{\prime(i)}\partial_Z\overline{\vartheta}_0^{(i)} = \frac{1}{Pr}\nabla_{\perp}^2\vartheta_1^{\prime(i)}, \tag{3.17}$$

$$\partial_\tau\overline{\vartheta}_0^{(i)} + \partial_Z\overline{(w_0^{\prime(i)}\vartheta_1^{\prime(i)})} = \frac{1}{Pr}\partial_Z^2\overline{\vartheta}_0^{(i)}, \tag{3.18}$$

where $D_t^{\perp}(\cdot) = \partial_t(\cdot) + \boldsymbol{u}\cdot\nabla_{\perp}(\cdot)$. The mean interior velocity field $\overline{\boldsymbol{u}}_0^{(i)}$ is zero and the mean momentum equation reduces to hydrostatic balance in the vertical, $\partial_Z\overline{p}_0^{(i)} = (\widetilde{Ra}/Pr)\overline{\vartheta}_0^{(i)}$.

The interior system is fourth order with respect to the large-scale vertical coordinate Z. Two boundary conditions are supplied by impenetrability such that $w_0^{\prime(i)}(0) = w_0^{\prime(i)}(1) = 0$. Although no Z derivatives with respect to $\vartheta_1^{\prime(i)}$ are present in (3.17), evaluation of this equation at the boundaries shows that the FT conditions $\vartheta_1^{\prime(i)}(0) = \vartheta_1^{\prime(i)}(1) = 0$ are satisfied implicitly for the fluctuating temperature. Evaluation of (3.16) at either the top or bottom boundary with the use of impenetrability shows that stress-free boundary conditions are implicitly satisfied as well since $\partial_Z\psi_0^{(i)}(0) = \partial_Z\psi_0^{(i)}(1) = 0$.

For the case of FT thermal boundary conditions, we have

$$\overline{\vartheta}_0^{(i)}(0) = 1 \quad \text{and} \quad \overline{\vartheta}_0^{(i)}(1) = 0 \quad \text{(FT)}. \tag{3.19a,b}$$

Thus, for the FT case the boundary layer corrections are identically zero and the above system is complete. Numerous investigations have used the above system of equations to investigate rapidly rotating convection in the presence of stress-free mechanical boundary conditions and have shown excellent agreement with direct numerical simulations (DNS) of the Navier–Stokes equations (Stellmach *et al.* 2014). In the presence of no-slip boundaries, order-one deviations in heat transfer are observed between simulations of the reduced equation set and DNS and laboratory experiments; these differences are thought to be the result of enhanced heat transfer due to Ekman pumping (Stellmach *et al.* 2014; Aurnou *et al.* 2015).

For the FF case the mean temperature boundary conditions become

$$\partial_Z\overline{\vartheta}_0^{(i)}(0) = -1 \quad \text{and} \quad \partial_Z\overline{\vartheta}_0^{(i)}(1) = -1 \quad \text{(FF)}. \tag{3.20a,b}$$

We further require $\partial_Z\vartheta_1^{\prime(i)}(0) = \partial_Z\vartheta_1^{\prime(i)}(1) = 0$; boundary layer corrections are therefore required since these conditions are not satisfied by (3.17). In the following two subsections we determine the magnitude of these boundary layer corrections.

3.2. *The middle layer equations*

The first non-trivial fluctuating middle layer momentum equation occurs at $O(\epsilon)$ to yield the thermal wind balance

$$\widehat{\boldsymbol{z}}\times\boldsymbol{u}_2^{\prime(m)} = -\nabla p_3^{\prime(m)} + \frac{\widetilde{Ra}}{Pr}\vartheta_2^{\prime(m)}\widehat{\boldsymbol{z}}, \tag{3.21}$$

such that $\nabla_{\perp}\cdot\boldsymbol{u}_2^{\prime(m)} = 0$ and $w_2^{\prime(m)} \equiv 0$. The mean velocity field $\overline{\boldsymbol{u}}_2^{(m)} \equiv 0$.

The leading-order temperature equation for the middle layer is

$$\partial_t\vartheta_2^{\prime(m)} + \boldsymbol{u}_0^{\prime(i)}(0)\cdot\nabla_{\perp}\vartheta_2^{\prime(m)} = \frac{1}{Pr}\nabla^2\vartheta_2^{\prime(m)}, \tag{3.22}$$

with corresponding boundary conditions

$$\partial_Z \vartheta_1'^{(i)}(0) + \partial_\xi \vartheta_2'^{(m)}(0) = 0, \quad \vartheta_2'^{(m)}(\xi \to \infty) \to 0. \tag{3.23}$$

We find the first non-trivial mean temperature to be of magnitude $O(\epsilon^5)$ (i.e. $\overline{\vartheta}^{(m)} = \epsilon^5 \overline{\vartheta}_5^{(m)} \neq 0$) and therefore omit any further consideration of this correction.

The first three orders of the stress-free mechanical boundary conditions along the bottom boundary become

$$\partial_Z \boldsymbol{u}_{0,\perp}'^{(i)}(0) = 0, \quad \partial_Z \boldsymbol{u}_{1/2,\perp}'^{(i)}(0) = 0, \quad \partial_Z \boldsymbol{u}_{1,\perp}'^{(i)}(0) + \partial_\xi \boldsymbol{u}_{2,\perp}'^{(m)}(0) + \partial_\eta \widetilde{\boldsymbol{u}}_0'^{(e)}(0) = 0. \tag{3.24a–c}$$

Thus, the first two orders of the interior velocity satisfy stress-free conditions on their own and therefore need no boundary layer correction. Here, we have rescaled the Ekman layer velocity according to $\boldsymbol{u}_{5/2}'^{(e)} = \epsilon^{5/2} \widetilde{\boldsymbol{u}}_0'^{(e)}$; this rescaling is simply highlighting the fact that the Ekman layer velocities are significantly weaker than those in the interior.

3.3. *The Ekman layer equations*

The Ekman layer equations have been studied in great detail in previous work (e.g. Greenspan 1968), so we simply state the leading-order continuity and momentum equations as

$$\nabla_\perp \cdot \widetilde{\boldsymbol{u}}_0'^{(e)} + \partial_\eta \widetilde{w}_{1/2}'^{(e)} = 0, \quad \widehat{\boldsymbol{z}} \times \widetilde{\boldsymbol{u}}_0'^{(e)} = \partial_\eta^2 \widetilde{\boldsymbol{u}}_0'^{(e)}, \tag{3.25a,b}$$

where $w_3'^{(e)} = \epsilon^3 \widetilde{w}_{1/2}'^{(e)}$. All of the mean Ekman layer variables can be shown to be zero. A key component in the present analysis that differs from previous work is the middle thermal wind layer that enters the Ekman layer solution via the stress-free boundary conditions (3.24*a–c*). On utilizing the thermal wind relations for the middle layer that follow from equation (3.21),

$$\partial_\xi u_2'^{(m)} = -\frac{\widetilde{Ra}}{Pr} \partial_y \vartheta_2'^{(m)}, \quad \partial_\xi v_2'^{(m)} = \frac{\widetilde{Ra}}{Pr} \partial_x \vartheta_2'^{(m)}, \tag{3.26a,b}$$

the stress-free boundary conditions along the bottom boundary can be written as

$$\partial_Z \boldsymbol{u}_{1,\perp}'^{(i)}(0) + \frac{\widetilde{Ra}}{Pr} \nabla^\perp \vartheta_2'^{(m)}(0) + \partial_\eta \widetilde{\boldsymbol{u}}_0'^{(e)}(0) = 0, \tag{3.27}$$

where $\nabla^\perp = (-\partial_y, \partial_x, 0)$. Solving the Ekman layer momentum equations for the horizontal components of the velocity field with the additional requirement that $(\widetilde{u}_0'^{(e)}, \widetilde{v}_0'^{(e)}) \to 0$ as $\xi \to \infty$, the continuity equation is then used to find the Ekman pumping velocity

$$\widetilde{w}_{1/2}'^{(e)} = \left[\partial_Z \zeta_1^{(i)}(0) + \frac{\widetilde{Ra}}{Pr} \nabla_\perp^2 \vartheta_2'^{(m)}(0) \right] \mathrm{e}^{-\eta/\sqrt{2}} \cos\left(\frac{\eta}{\sqrt{2}} \right). \tag{3.28}$$

Thus, vertical velocities of magnitude $O(\epsilon^3)$ are induced by FF thermal boundary conditions and result from both finite viscous stresses within the fluid interior and horizontal variations of the temperature within the middle layer. This finding is closely analogous to the Ekman pumping effect first reported by Hide (1964) for shallow layer

quasi-geostrophic flow in the presence of lateral temperature variations along a free surface. Evaluating (3.28) at $\eta = 0$ provides a parameterized boundary condition for the effects of Ekman pumping.

The small magnitude of the Ekman pumping velocity (3.28) results in very weak $O(\epsilon^5)$ temperature fluctuations within the Ekman layer. Because of this, the dominant correction of the FF thermal boundary conditions occurs within the middle layer and we do not consider the Ekman layer temperature any further.

3.4. *Synthesis*

The thermal boundary layer correction given by (3.23) is passive in the sense that $\vartheta_2^{\prime(m)}$ can be calculated *a posteriori* with knowledge of $\vartheta_1^{\prime(i)}$. Thus, the leading-order interior dynamics is insensitive to the thermal boundary conditions. The Ekman layer analysis shows that the first six orders of the interior vertical velocity satisfy the impenetrable mechanical boundary conditions $w_i^{\prime(i)}(0) = 0$, for $i = 0, \ldots, 5/2$. At $O(\epsilon^3)$ we have the Ekman pumping boundary conditions

$$w_3^{\prime(i)}(0) = -w_3^{\prime(m)}(0) - \partial_Z \zeta_1^{(i)}(0) - \frac{\widetilde{Ra}}{Pr}\nabla_\perp^2 \vartheta_2^{\prime(m)}(0), \tag{3.29}$$

where we have used the Ekman pumping relation (3.28) evaluated at $\eta = 0$. From the standpoint of linear theory, the first correction to the critical Rayleigh number will therefore occur at $O(\epsilon^3)$; this explains the linear behaviour previously discussed in § 2. Although the above velocity correction is asymptotically weak, we note that it may be possible to identify this additional circulation in DNS studies by employing the method outlined by Kunnen, Clercx & Geurts (2013).

4. Discussion

In light of the boundary layer analysis, we conclude that the leading-order quasi-geostrophic dynamics is described by equations (3.15)–(3.18) for both FT and FF thermal boundary conditions. Indeed, inspection of the system shows that it is invariant under the following rescaling of the Rayleigh numbers and temperature variables:

$$\widetilde{Ra}_{FT} = \frac{\widetilde{Ra}_{FF}}{Nu}, \quad \vartheta_{1,FT}^{\prime(i)} = Nu\,\vartheta_{1,FF}^{\prime(i)}, \quad \overline{\vartheta}_{0,FT}^{(i)} = Nu\,\overline{\vartheta}_{0,FF}^{(i)}. \tag{4.1a–c}$$

Integration of the time-averaged mean heat equation with respect to Z yields

$$Pr\overline{(w_0^{\prime(i)}\vartheta_{1,FT}^{\prime(i)})} = \partial_Z \overline{\vartheta}_{0,FT}^{(i)} + Nu \quad \text{(FT)}, \tag{4.2}$$

$$Pr\overline{(w_0^{\prime(i)}\vartheta_{1,FF}^{\prime(i)})} = \partial_Z \overline{\vartheta}_{0,FF}^{(i)} + 1 \quad \text{(FF)}, \tag{4.3}$$

for the FT and FF cases respectively. The appropriate thermal boundary conditions have been applied at $Z = 0$ in the above relations. Taking either (4.2) or (4.3) and utilizing (4.1a–c) shows that the mean interior temperature gradient is described by identical equations for the two cases.

The above results indicate that the findings of previous work on low-Rossby-number convection employing FT thermal boundary conditions can be accurately applied to the case of FF thermal boundary conditions by use of the rescalings given by (4.1a–c).

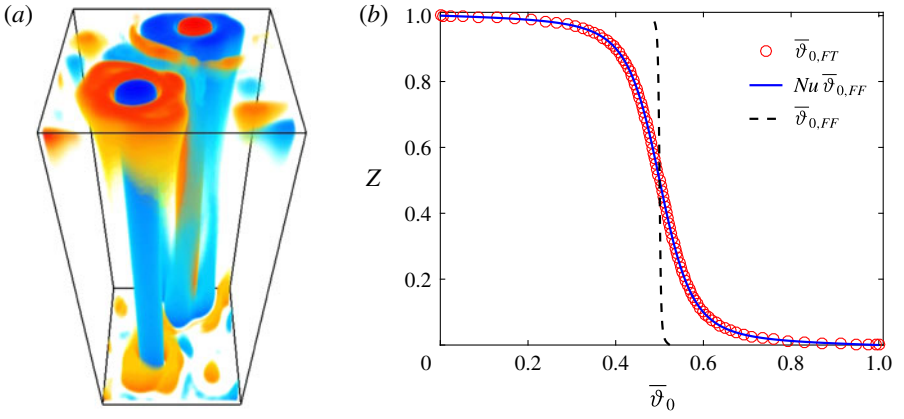

FIGURE 2. (*a*) An example volumetric rendering of the temperature perturbation from a simulation of the quasi-geostrophic convection equations showing the 'convective Taylor column' (CTC) regime. (*b*) Mean temperature profiles obtained with both FT (solid blue) and FF (dashed black) boundary conditions, and the rescaled FF temperature profile (red open circles). The parameters are $Pr = 7$, $\widetilde{Ra}_{FT} = 46.74$, $\widetilde{Ra}_{FF} = 1000$ and $Nu = 21.39$.

Julien *et al.* (2012*b*) identified four flow regimes that occur in rapidly rotating convection as a function of the Prandtl and (FT) Rayleigh numbers. The so-called 'convective Taylor column' (CTC) regime is distinguished by coherent vertically aligned convective structures that span the depth of the fluid. Figure 2(*a*) shows a volumetric rendering of the temperature perturbation for $Pr = 7$ and $\widetilde{Ra}_{FT} = 46.74$, or $\widetilde{Ra}_{FF} = 1000$ and $Nu = 21.39$; this case was computed explicitly with FF thermal boundary conditions. The CTC regime occurs over the FT Rayleigh number range of $20 \lesssim \widetilde{Ra}_{FT} \lesssim 55$, corresponding to an FF Rayleigh number range of $82 \lesssim \widetilde{Ra}_{FF} \lesssim 1656$ (e.g. see Nieves, Rubio & Julien 2014). Figure 2(*b*) shows mean temperature profiles obtained utilizing the FT and FF thermal boundary conditions, along with the remapped FF mean temperature profile. The Nusselt number $Nu = 21.39$ corresponds to a mean temperature difference of 0.0468 between the top and bottom boundaries for the FF case. Given that the mapping defined by (4.1*a*–*c*) is independent of the Prandtl number, we note that the rescaling shown in figure 2(*b*) can be carried out for any Prandtl number.

Of particular interest in convection studies is the dependence of the heat transfer scaling on the strength of the thermal forcing input via Nusselt–Rayleigh number scalings of the form $Nu \sim \widetilde{Ra}_{FT}^{\alpha}$. With the rescaling given in (4.1*a*–*c*) the FF equivalent of this relation becomes $Nu \sim \widetilde{Ra}_{FF}^{\beta}$, where $\beta = \alpha/(\alpha + 1)$. For the CTC regime the exponent is $\alpha \approx 2.1$ (Julien *et al.* 2012*b*), yielding $\beta \approx 0.68$. Additionally, the final regime of geostrophic turbulence achieves a dissipation-free scaling law with $\alpha = 3/2$ such that $\beta = 3/5$ (Julien *et al.* 2012*a*). Similarly, the dependence of all other variables of interest on the Rayleigh number (e.g. mean temperature gradient, vorticity, etc.) can also be remapped to the case of FF thermal boundary conditions.

5. Conclusion

In this work we have shown that the leading-order dynamics of rapidly rotating convection in a plane layer geometry are equivalent for both FT and FF thermal boundary conditions. Fixed flux thermal boundary conditions give rise to a double

boundary layer structure in the limit of rapid rotation that induces a vertical mass flux, or Ekman pumping, that is given explicitly by (3.28). The Ekman pumping velocity is asymptotically weak, however, and we conclude that all previous work employing FT thermal boundary conditions also accurately describes FF thermal boundary conditions as long as the Rossby number remains small. Practically speaking, the influence of rotation can be expected to be strong when $Ro \lesssim 0.1$ (e.g. Vorobieff & Ecke 2002; Horn & Shishkina 2015). Our findings imply that the reduced quasi-geostrophic model defined by (3.15)–(3.18) applies to both FT and FF thermal boundary conditions within the regime of asymptotic validity, i.e. $Ro \sim E_H^{1/3} \ll 1$, $E_H \ll Pr$ and $\widetilde{Ra} \lesssim O(E_H^{-1/3})$ (Julien *et al.* 2012*a*). For $Pr = O(E_H)$, rapid oscillations occur such that the inertia can be large enough to balance the Coriolis and pressure gradient forces (Zhang & Roberts 1997), whereas the bound on $\widetilde{Ra}$ further ensures that the Rossby number remains small.

The influence of both thermal and mechanical boundary conditions on non-rotating convection has received significant attention (e.g. Johnston & Doering 2009; van der Poel *et al.* 2014). For the case of rotating convection, plane layer investigations have shown that both no-slip and stress-free mechanical boundary conditions yield similar convective dynamics (King *et al.* 2009; Schmitz & Tilgner 2010), though the presence of Ekman pumping for no-slip boundary conditions is now known to significantly enhance heat transfer in comparison to stress-free simulations (Kunnen, Clercx & Geurts 2006; Stellmach *et al.* 2014). To date, studies investigating the role of thermal boundary conditions on nonlinear rotating convection have been focused solely on spherical geometries. Zhang & Gubbins (1993) showed that convection cells in a rotating spherical shell can resonate with inhomogeneous (spatially varying) temperature boundary conditions. A subsequent investigation by Davies, Gubbins & Jimack (2009) has shown that resonance is dependent upon both the rotation rate and the spatial scale of the thermal anomaly along the outer boundary, with resonance vanishing when the scale of the temperature variation is comparable to the most unstable wavelength and the rotation rate of the system is large. Our asymptotic analysis complements these previous numerical findings and rigorously shows that any horizontal thermal variation along the boundaries that varies on the scale of the convection, as allowed for with FF thermal boundary conditions, has no leading-order influence on the interior convection. However, we note that resonance can occur when the spatial scale of the thermal anomaly is comparable to the vertical scale of convection (Davies *et al.* 2009); this is the mechanism likely to cause significant changes in the magnetic and velocity fields observed in spherical dynamo simulations with FF boundary conditions (Sakuraba & Roberts 2009, 2011).

Acknowledgements

This work was supported by the National Science Foundation under grants EAR no. 1320991 (M.A.C. and K.J.), EAR CSEDI no. 1067944 (K.J. and P.M.) and DMS EXTREEMS no. 1407340 (D.D.).

References

AHLERS, G., GROSSMAN, S. & LOHSE, D. 2009 Heat transfer and large scale dynamics in turbulent Rayleigh–Bénard convection. *Rev. Mod. Phys.* **81**, 503–537.

AURNOU, J. M., CALKINS, M. A., CHENG, J. S., JULIEN, K., KING, E. M., NIEVES, D., SODERLUND, K. M. & STELLMACH, S. 2015 Rotating convective turbulence in Earth and planetary cores. *Phys. Earth Planet. Inter* **246**, 52–71.

Calkins, M. A., Julien, K. & Marti, P. 2013 Three-dimensional quasi-geostrophic convection in the rotating cylindrical annulus with steeply sloping endwalls. *J. Fluid Mech.* **732**, 214–244.

Chandrasekhar, S. 1961 *Hydrodynamic and Hydromagnetic Stability*. Oxford University Press.

Chapman, C. J. & Proctor, M. R. E. 1980 Nonlinear Rayleigh–Bénard convection between poorly conducting boundaries. *J. Fluid Mech.* **101**, 759–782.

Cheng, J. S., Stellmach, S., Ribeiro, A., Grannan, A., King, E. M. & Aurnou, J. M. 2015 Laboratory–numerical models of rapidly rotating convection in planetary cores. *Geophys. J. Intl* **201**, 1–17.

Davies, C., Gubbins, D. & Jimack, P. 2009 Convection in a rotating spherical fluid shell with an imposed laterally varying thermal boundary condition. *J. Fluid Mech.* **641**, 335–358.

Dowling, T. E. 1988 Rotating Rayleigh–Bénard convection with fixed flux boundaries. In *Summer Study Program in Geophysical Fluid Dynamics, Woods Hole Oceanographic Institution Technical Report*, pp. 230–247.

Ecke, R. E. & Niemela, J. J. 2014 Heat transport in the geostrophic regime of rotating Rayleigh–Bénard convection. *Phys. Rev. Lett.* **113**, 114301.

Greenspan, H. P. 1968 *The Theory of Rotating Fluids*. Cambridge University Press.

Heard, W. B. & Veronis, G. 1971 Asymptotic treatment of the stability of a rotating layer of fluid with rigid boundaries. *Geophys. Fluid Dyn.* **2** (1), 299–316.

Hide, R. 1964 The viscous boundary layer at the free surface of a rotating baroclinic fluid. *Tellus* **16**, 523–529.

Horn, S. & Shishkina, O. 2015 Toroidal and poloidal energy in rotating Rayleigh–Bénard convection. *J. Fluid Mech.* **762**, 232–255.

Hurle, D. T. J., Jakeman, E. & Pike, E. R. 1967 On the solution of the Bénard problem with boundaries of finite conductivity. *Proc. R. Soc. Lond.* A **296**, 469–475.

Johnston, H. & Doering, C. R. 2009 Comparison of turbulent thermal convection between conditions of constant temperature and constant flux. *Phys. Rev. Lett.* **102**, 064501.

Julien, K., Knobloch, E., Rubio, A. M. & Vasil, G. M. 2012*a* Heat transport in low-Rossby-number Rayleigh–Bénard convection. *Phys. Rev. Lett.* **109**, 254503.

Julien, K., Legg, S., McWilliams, J. & Werne, J. 1996 Rapidly rotating turbulent Rayleigh–Bénard convection. *J. Fluid Mech.* **322**, 243–273.

Julien, K., Rubio, A. M., Grooms, I. & Knobloch, E. 2012*b* Statistical and physical balances in low Rossby number Rayleigh–Bénard convection. *Geophys. Astrophys. Fluid Dyn.* **106** (4–5), 392–428.

King, E. M., Stellmach, S., Noir, J., Hansen, U. & Aurnou, J. M. 2009 Boundary layer control of rotating convection systems. *Nature* **457**, 301–304.

Kunnen, R. P. J., Clercx, H. J. H. & Geurts, B. J. 2006 Heat flux intensification by vortical flow localization in rotating convection. *Phys. Rev.* E **74**, 056306.

Kunnen, R. P. J., Clercx, H. J. H. & Geurts, B. J. 2013 The structure of the sidewall boundary layers in confined rotating Rayleigh–Bénard convection. *J. Fluid Mech.* **727**, 509–532.

Liu, Y. & Ecke, R. E. 1997 Heat transport scaling in turbulent Rayleigh–Bénard convection: effects of rotation and Prandtl number. *Phys. Rev. Lett.* **79** (12), 2257–2260.

Nayfeh, A. H. 2008 *Perturbation Methods*. John Wiley & Sons.

Nieves, D., Rubio, A. M. & Julien, K. 2014 Statistical classification of flow morphology in rapidly rotating Rayleigh–Bénard convection. *Phys. Fluids* **26**, 086602.

van der Poel, E. P., Ostilla-Mónico, R., Verzicco, R. & Lohse, D. 2014 Effect of velocity boundary conditions on the heat transfer and flow topology in two-dimensional Rayleigh–Bénard convection. *Phys. Rev.* E **90**, 013017.

Sakuraba, A. & Roberts, P. H. 2009 Generation of a strong magnetic field using uniform heat flux at the surface of the core. *Nature Geosci.* **2**, 802–805.

Sakuraba, A. & Roberts, P. H. 2011 On thermal driving of the geodynamo. In *The Earth's Magnetic Interior* (ed. E. Petrovskỳ, D. Ivers, T. Harinarayana & E. Herrero-Bervera), pp. 117–129. Springer.

Schmitz, S. & Tilgner, A. 2010 Transitions in turbulent rotating Rayleigh–Bénard convection. *Geophys. Astrophys. Fluid Dyn.* **104** (5–6), 481–489.

SPRAGUE, M., JULIEN, K., KNOBLOCH, E. & WERNE, J. 2006 Numerical simulation of an asymptotically reduced system for rotationally constrained convection. *J. Fluid Mech.* **551**, 141–174.

STELLMACH, S., LISCHPER, M., JULIEN, K., VASIL, G., CHENG, J. S., RIBEIRO, A., KING, E. M. & AURNOU, J. M. 2014 Approaching the asymptotic regime of rapidly rotating convection: boundary layers versus interior dynamics. *Phys. Rev. Lett.* **113**, 254501.

STEVENS, R. J. A. M., CLERCX, H. J. H. & LOHSE, D. 2013 Heat transport and flow structure in rotating Rayleigh–Bénard convection. *Eur. J. Mech. (*B-*Fluids)* **40**, 41–49.

TAKEHIRO, S.-I., ISHIWATARI, M., NAKAJIMA, K. & HAYASHI, Y.-Y. 2002 Linear stability of thermal convection in rotating systems with fixed heat flux boundaries. *Geophys. Astrophys. Fluid Dyn.* **96** (6), 439–459.

VOROBIEFF, P. & ECKE, R. E. 2002 Turbulent rotating convection: an experimental study. *J. Fluid Mech.* **458**, 191–218.

ZHANG, K. & ROBERTS, P. H. 1997 Thermal inertial waves in a rotating fluid layer: exact and asymptotic solutions. *Phys. Fluids* **9** (7), 1980–1987.

ZHANG, K. K. & GUBBINS, D. 1993 Convection in a rotating spherical fluid shell with inhomogeneous temperature boundary condition at infinite Prandtl number. *J. Fluid Mech.* **250**, 209.